DETERMINATION OF SPECIFIC RAIN ATTENUATION USING DIFFERENT TOTAL CROSS SECTION MODELS FOR SOUTHERN AFRICA

S.J. Malinga*, P.A. Owolawi and T.J.O. Afullo*****

** Dept. of Electrical Engineering, Mangosuthu University of Technology, P. O. Box 12363, Jacobs, Durban,4026, South Africa. E-mail: senzo@mut.ac.za*
*** Dept. of Electrical Engineering, Mangosuthu University of Technology, P. O. Box 12363, Jacobs, Durban,4026, South Africa. E-mail: owolawi@mut.ac.za*
**** Discipline of Electrical, Electronic and Computer Engineering, University of KwaZulu-Natal, Durban, South Africa E-mail: afullot@ukzn.ac.za*

Abstract: In terrestrial and satellite line-of-sight links, radio waves propagating at Super High Frequency and Extremely High Frequency bands through rain undergo attenuation (absorption and scattering). In this paper, the specific attenuation due to rain is computed using different total cross section models, while the raindrop size distribution is characterised for different rain regimes in the frequency range between 1 and 100 GHz. The Method of Moments is used to model raindrop size distributions, while different extinction coefficients are used to compute the specific rain attenuation. Comparison of theoretical results of the existing models and the proposed models against experimental outcomes for horizontal and vertical polarizations at different rain rates are presented.

Keywords: Method of moments, microwave attenuation, millimeter wave attenuation, rain attenuation, rainfall regimes, rain types, satellite communication, terrestrial communication, fade margin.

1. INTRODUCTION

The advantages offered by Super High Frequency (SHF) and Extremely High Frequency (EHF) bands such as large bandwidth, small antenna size, and easy installation or deployment have motivated the interest of researchers to study various factors that prevent optimum utilization of these bands. Factors such as cloud, hail, fog, snow, ice crystals, and rain degrade terrestrial and satellite link performance at these frequencies. Rain fade remains the dominant factor in signal fading over satellite and terrestrial links, especially in the tropical and sub-tropical regions like South Africa. In this paper, the focus is on signal attenuation due to absorption and scattering by rain. While other types of hydrometeors such as water vapour, snowfall, and hail are considered secondary deleterious factors to link design at these frequency bands, attenuation due to rain is a fundamental quantity in the estimation of signal degradation in the presence of precipitation for terrestrial and satellite links. As presented in several articles, a simple power-law relationship of specific rain attenuation as given in equation (1) is widely used, and the values of the coefficient parameters k and α are listed in the International Telecommunication Union Recommendation ITU-R P.838.3 [1].

$$\gamma_R = kR^{\alpha} \tag{1}$$

Here R (mm/h) is the rain rate and k and α are constants at a given frequency. It is evident from several contributors [2, 3, 4] that k and α vary with the raindrop size distribution (DSD). It is observed as well that the rain DSD is location and climate dependent.

In order to account for the degree of rain attenuation or rain fade in a link, two methods are often considered: the direct method (which refers to direct measurements at the receiver using a spectrum analyzer), and the statistical method (which involves rain rate and raindrop size measurement). The rain rate and raindrop size measurements allow for the estimation of rain attenuation in a cost-effective way as compared with the direct method. Regional and global efforts have been made to obtain suitable distribution functions and related parameters for the raindrop size distribution (DSD). The early DSD models were based on exponential [5] distribution functions, which poorly represented the very small and very large raindrops. The other distribution functions that have been suggested are the Lognormal [2, 6], the Weibull [7, 8], and the gamma [9] distribution functions. There are several ways of fitting measured DSD data, of which the method of moments [10] and maximum likelihood estimation [11] are the most popularly used by many authors. While DSD measurement campaigns have been reported over a considerable period of time in West Africa [2, 12], less attention has been invested in this regard in Southern Africa [13, 14].

One of the aims of this paper is to give a report on the current DSD modelling for the South African region and its application using different extinction cross section models. The resulting fitted DSD is integrated over the scattering cross section to calculate the specific attenuation due to rain. In order to estimate the total cross sectional area of raindrops, the choice of rain shape is the key parameter. Morrison and Cross [15] fitted the drop

shape with a spheroidal model, using a least-squares method. The contribution of Pruppacher and Pitter [16], presented theoretical results of raindrops at different sizes, while Li *et al.* [17, 18] further simplified Pruppacher and Pitter's model, with the expression:

$$r = a(1-v_1)\left[f_0(\theta) + \frac{v_1}{1-v_1} f_1(\theta)\right] = \begin{Bmatrix} a(1-v_1)\left[1 + \frac{v_1}{1-v_1} sin^2\theta\right], \ 0 \le \theta \le \pi/2 \\ a(1-v_2)\left[1 + \frac{v_2}{1-v_2} sin^2\theta\right], \ \pi/2 \le \theta \le \pi \end{Bmatrix} \quad (2)$$

where,

$$a = 1.111582a_0 \quad (3a)$$

$$v_1 = 1.375447\times10^{-2} + 6.543960\times10^{-2}a \quad (3b)$$

$$v_2 = -7.239211\times10^{-2} + 1.827561\times10^{-1}a \quad (3c)$$

$$f_0(\theta) = 1 - \frac{v_2 - v_1}{1-v_1} H(\theta - \frac{\pi}{2}) \quad (3d)$$

$$f_1(\theta) = \left[1 + \frac{v_2 - v_1}{1-v_1} H(\theta - \frac{\pi}{2})\right] sin^2\theta \quad (3e)$$

Here a_0 denotes the mean raindrop radius, theoretically given as 0.25 mm to 3.00 mm with an incremental interval of 0.25 mm, and $H(\theta)$ denotes the step function. Equations (2) to (3) represent the spherical raindrop size model. Another approach with a new formula was presented in reference [19] - in which case the scattered electromagnetic fields were deemed due to spheroidal raindrops. Considering spheroidal raindrop scatterers, the surface of the drops is described by:

$$r = \frac{a}{\sqrt{1 - v.sin^2\theta}} \approx a\left[1 + \frac{1}{2} v sin^2\theta\right] \quad (4)$$

where $v = 1 - ((a/b)^2)$, and a and b represent the raindrop's minor and major semi-axes respectively, and are measured in centimeters. In [19] Oguchi's method was used to obtain a and b from the mean drop size radius $\bar{a}$ that was developed to determine the specific rainfall attenuation. Oguchi [20] assumed that:

$$ab^2 = \bar{a}^3 \quad ; \quad \frac{a}{b} = \left(1 - \frac{4.1}{4.5}\bar{a}\right) \quad (5)$$

The other method presented in [19] is that of Morrison and Cross [15], which assumes that:

$$ab^2 = \bar{a}^3 \quad ; \quad \frac{a}{b} = 1 - \bar{a} \quad (6)$$

The parameters obtained using the method of Morrison and Cross have shown reasonably consistent results when considering larger raindrops as opposed to that proposed by Oguchi [20]. This paper thus uses the aforementioned total scattering cross section of Morrison and Cross [15], alongside the Pruppacher and Pitter model [16] as well as the Mie model, to compute the specific attenuation due to rain for Southern Africa.

2. DISDROMETER DATA COLLECTION

For the purpose of this submission, two-year DSD data was collected using the Joss-Waldvogel RD-80 disdrometer (JWD) at an integration time of one minute. This equipment is placed at latitude $30^0 58$ E and longitude $29^0 52$ S atop the Electrical, Electronic, and Computer Engineering building, University of KwaZulu-Natal, at an altitude of 139.7 m above sea-level. It measures raindrop diameters in the range of 0.3 mm to 5 mm in 20 different bins, with the accuracy of ±5%. The expression used to estimate the measured rain rate (mm/hr) by the equipment is presented in the JWD manual as [21]:

$$R = \left(\frac{3600\pi}{6ST} \sum_{i=1}^{20} D_i^3 n_i\right) \quad (7)$$

while the measured DSD, or $N(D_i)$, is given by [21]:

$$N(D_i) = \frac{n_i \times 10^6}{v(D_i) \times S \times T \times \Delta D_i} \quad (8)$$

Note that $S = 5000\ mm^2$, $T = 60\ s$, $v(D_i)$ is the terminal velocity, estimated using the Gunn and Kinzer approach, and n_i is the number of drops. With the nature of rain distribution in Southern Africa, the rain rate is used to classify the raindrop size distribution models into four classes:

- Drizzle ($R < 5mm/hr$)
- Widespread ($5mm/hr \le R < 10\ mm/hr$)
- Shower ($10\ mm/hr \le R < 40\ mm/hr$)
- Thunderstorm ($R \ge 40\ mm/hr$)

The rain rate can be estimated from the modelled $N(D_i)$ for each class of rain rate type, given by the expression:

$$R = 1.8849\times10^{-3} \sum_{i=1}^{20} D_i^3 v(D_i) N(D_i) \Delta D_i \quad (9)$$

In the comparative studies of the measured $N(D_i)$ and modelled $N(D_i)$, the root mean square error (RMSE)% is defined as:

$$RMSE\ (\%) = \left[\frac{1}{n}\sum_{i=1}^{n} [Measured - Modelled]^2\right]^{1/2} \times 100 \quad (10)$$

3. THE METHOD OF MOMENTS

In this paper, the 3rd, 4th, and 6th order moments are employed to determine the three Lognormal DSD parameters because of its simplicity and immediate physical interpretation of the Lognormal parameters. The nth order moment is defined as:

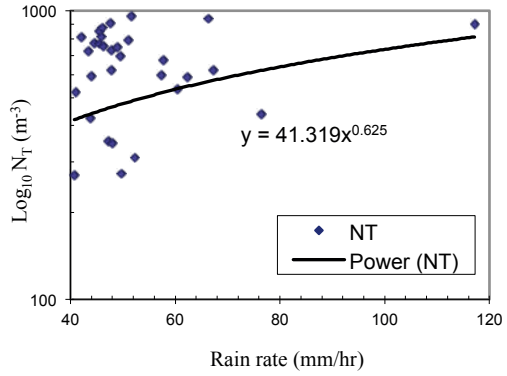

(a)

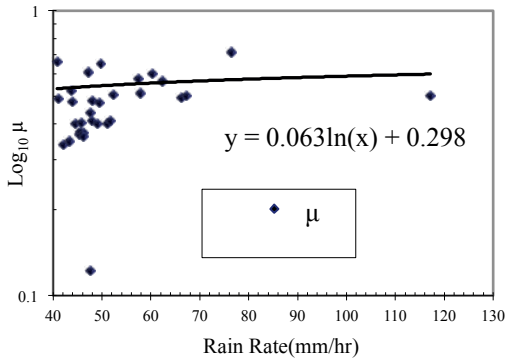

(b)

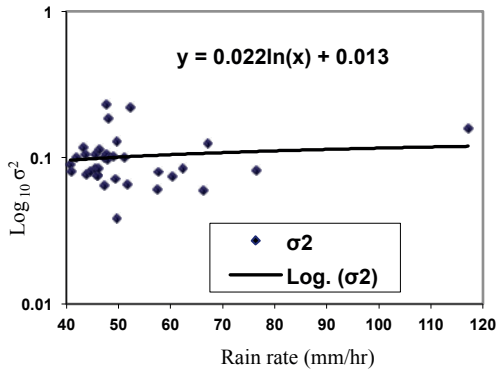

(c)

Figure 1: Scattergrams of estimated Lognormal parameters (a) N_T (b) μ and (c) σ^2, versus the rain rate for the thunderstorm rain type

$$M_n = \int_0^\infty N(D)(D)^n dD \tag{11}$$

For the Lognormal DSD, the $N(D_i)$ model is given as:

$$N(D) = \frac{N_T}{\sigma D\sqrt{2\pi}} exp\left[-\frac{(lnD-\mu)^2}{2\sigma^2}\right] \tag{12}$$

where D is the raindrop diameter, and N_T, μ, and σ are the three Lognormal parameters. To simplify equation (11) in the form of equation (12), the integral rain parameters are approximated by *x-th, y-th* and *z-th* moments of the DSD where x, y, and z are non-integer. Then equation (11) is equivalent to:

$$M_x = N_T exp\left(x\mu + \frac{1}{2}x^2\sigma^2\right) \tag{13}$$

M_y and M_z are similar to equation (13). Taking L_x to be the natural logarithm of M_x, the Lognormal DSD parameters are calculated as [10]:

$$N_T = exp[(24L_3 - 27L_4 - 6L_6)/3] \tag{14a}$$

$$\mu = (-10L_3 + 13.5L_4 - 3.5L_6)/3 \tag{14b}$$

$$\sigma^2 = (2L_3 - 3L_4 + L_6)/3 \tag{14c}$$

Fig. 1 presents logarithmic scattergrams of Lognormal DSD parameters versus rain rate for the thunderstorm rain type. These parameters are derived from equations (13) and (14). For the other rain types such as drizzle, widespread and shower, Table 1 and expressions presented in equation (15) give details of Lognormal DSD parameters and their coefficients for the Southern African region as summarized in the expressions below:

$$N_T = a_0 R^{b_0} \tag{15a}$$
$$\mu = A_\mu + B_\mu lnR \tag{15b}$$

3.1 Application of Rainfall Regimes

It has been established that the raindrop size distribution varies considerably for different types of rainfall regimes or classes. These rainfall classes, as defined in section 2, are: drizzle, widespread, shower and thunderstorm. The corresponding parameters of their Lognormal distributions are shown in Table 1. A general distribution model has often been used by many researchers. However, there is a notable difference in the specific attenuation due to rain produced by the general model, hence the need to develop regime-specific rain attenuation models [22, 23].

3.2. Comparative studies of DSD models between Southern and West Africa

The performance test analysis of the proposed Lognormal model and its counterpart from West Africa [22] are evaluated using equation (10). The comparison is done by substituting the coefficients in Table 1a and 1b into equation (15) with measurements carried out in Durban as discussed in section 2 of this paper.

The RMSE model performance test is carried out by taking at least three rain rate samples of each rain type, with the average RMSE in percentage then calculated for each rain type. The proposed Lognormal model performs better than its counterparts across all the rain regimes. The test results agree with RMSE results presented in [23].

Table 1a: Coefficients of Lognormal DSD parameters in equation (15) for Southern Africa

Rain Type	a_0	b_0	A_μ	B_μ	A_σ	B_σ
Drizzle	212.3	0.387	-0.281	0.131	0.086	0.013
Shower	258.3	0.095	-0.321	0.242	0.072	0.005
Wide spread	322.4	0.102	-0.392	0.249	0.083	-0.003
Thunder storm	41.3	0.625	0.299	0.063	0.014	0.022
General model	220.0	0.392	-0.267	0.137	0.077	0.010

Table 1b: Coefficients of Lognormal DSD parameters for West Africa [22]

Rain Type	a_0	b_0	A_μ	B_μ	A_σ	B_σ
Drizzle	718.00	0.399	-0.51	0.128	0.038	0.013
Shower	137.00	0.370	-0.41	0.234	0.223	-0.03
Wide spread	264.00	-0.23	-0.47	0.174	0.161	0.018
Thunder storm	63.00	0.491	-0.18	0.195	0.209	-0.03
General model	108.00	0.363	-0.20	0.199	0.137	-0.01

Table 2: Error analysis (RMSE in %) of the proposed Lognormal model and West Africa model

Rain Type	Lognormal model (West Africa)	Proposed Lognormal Model
Drizzle	8.01	4.03
Shower	9.85	4.53
Widespread	10.98	5.01
Thunderstorm	13.15	6.95
General	11.49	4.14

Table 3: Comparison of rain attenuation for P-P and MC model against the Mie model at different rain rates at 100 GHz

Rain Type	Attenuation Percentage Difference (%) between Mie and P-P and MC-model	
	P-P model	MC model
Drizzle	4.36	8.98
Widespread	5.96	10.81
Shower	15.35	17.83
Thunderstorm	30.95	31.47

The slight deviations of RMSE values recorded are due to the optimum best fit function employed (such as linear, power law, and exponential fits) in [23] and the averaged RMSE calculated for each rain type. The summary of the RMSE performance test is presented in Table 2.

4. SCATTERING PROPERTIES OF DISTORTED RAINDROPS

The investigation and successful prediction of the attenuation of plane electromagnetic waves caused by a rainy medium involves an assumption of a particular physical model for the raindrop shape. The total scattering cross-section (extinction cross-section) of the raindrop depends to a great deal on this physical model. Many researchers have adopted a simple approach that assumes raindrops to be spherical in shape and employed the Mie theory to obtain the specific attenuation due to rain. However, it has been established through photographic measurements [24, 25] that realistic raindrops become oblate spheroidal in shape as the drop size gets larger. Raindrops of fairly large size experience severe distortion, and as such, they are no longer spheroidal in shape but look like hamburgers [26, 27]. This loss of shape is accompanied by a loss of symmetry along their axes. The assumption that raindrops are spherical, as adopted by many researchers, is therefore valid only for small raindrops.

4.1 Scattering Coefficients

Scattering coefficients can be obtained by considering different orders of approximations, with the zeroth-order scattering from the spheroid representing the Mie scattering from a sphere [19]. Li *et al* [19] discuss two approaches for obtaining the first-order scattering approximation. The first approach is to modify the scattering coefficients $S_n^a(a_e)$ and $S_n^b(a_e)$ through the use of an effective radius of the spheroid, while the second approach involves the modification of the spherical vector wave functions to the spheroidal ones.

The second approach involves lengthy and error-prone calculations hence it is much easier to execute the first approach. This approach suggests that the variability of the raindrop shape merely translates to the variability of the effective raindrop radius. For spherical raindrops, the scattering coefficients are expressed in terms of the mean drop radius of the sphere.

The following equation was thus considered to represent the surface of an arbitrarily-distorted scatterer [19]:

$$r = a[1 + vf(\theta', \phi')] \tag{16}$$

where θ' and ϕ' represent the zenith and the azimuth angles of the incident waves at which reflection occurs. The above equation clearly shows that for small values of v, $r \approx a$. This implies that the second term in the above equation represents a distortion with respect to a sphere of radius a. It can therefore be considered that the term $a[1 + vf(\theta', \phi')]$ represents the effective radius a_e of an arbitrarily-shaped scatterer [19].

The scattering coefficients are thus given by [18, 19]:

$$S_n^a = -\frac{j_n(\zeta D)[Dj_n(D)]' - j_n(D)[\zeta D j_n(\zeta D)]'}{j_n(\zeta D)\left[Dh_n^{(2)}(D)\right]' - h_n^{(2)}(D)[\zeta D j_n(\zeta D)]'} \quad (17)$$

$$S_n^b = -\frac{j_n(D)[\zeta D j_n(\zeta D)]' - \zeta^2 j_n(\zeta D)[D j_n(D)]'}{h_n^{(2)}(D)[\zeta D j_n(\zeta D)]' - \zeta^2 j_n(\zeta D)\left[Dh_n^{(2)}(D)\right]'} \quad (18)$$

and the parameter D is given by:

$$D = k_0 a[1 + vf(\alpha, 0)] \quad (19)$$

where k_0 is the free space wave number and α is the incidence angle.

The parameter D is analogous to the size parameter commonly used in the Mie calculations. Once the shape of the raindrops is known the scattering coefficients can be determined. The extinction (total) cross-section is then calculated based on the different shapes for different models as follows [15, 20]:

$$Q_{ext} = -\frac{2\pi}{k_0^2} Re \sum_{n=1}^{\infty}(2n+1)[S_n^a(a_e) + S_n^b(a_e)] \quad (20)$$

where a_e is the effective raindrop radius given by [20, 21]:

$$a_e = \frac{a}{\sqrt{1-v}} \quad (21)$$

4.2 Total Scattering Cross Section

In this paper, the total scattering cross-section is evaluated and plotted against the mean raindrop radius for three different models. We consider the Morrison and Cross (M-C) model for spheroidal raindrops; the Pruppacher and Pitter (P-P) model for raindrops of any size and shape; and the Mie model for spherical rain drops. The first two models are polarization dependent while the third model is polarization independent. In order to evaluate the effect of polarization using the three total cross-section models, the following six frequencies are used: 7.8 GHz, 13.6 GHz, 19.5 GHz, 34.8 GHz, 140 GHz, and 245.5 GHz. The corresponding complex refractive indices of water at a temperature of 20 degrees Celsius using the method of Liebe *et al* for these frequencies are: (8.3614+*i*1.697), (7.5307+*i*2.4231), (6.7189+*i*2.7566), (5.2534+*i*2.8091), (2.9701+*i*1.5635), and (2.5945+*i*1.1046), respectively.

Fig. 2 shows that the different models are in agreement in terms of the extinction cross section for small raindrop diameters and lower frequencies. As the drop diameter increases, a noticeable difference is observed among the models. The Mie model gives the lowest values of extinction cross-section while the higher values are obtained from the M-C and P-P models due to the degree of the raindrops' distortion. The results confirm the inability of the Mie model to realistically represent the raindrop shape, reducing it to a smaller sized sphere in comparison with the realistic spheroid of the M-C and P-P models. Figure 2 confirms that different polarizations have different effects on the total cross section. The horizontally-polarized wave records a larger value of total cross-section than its vertical counterpart.

By using the percentage difference between the P-P model and the Mie model at 7.8 GHz, it confirmed that at lower diameters, the percentage difference is minimal. At a diameter of 2 mm, it is seen that the percentage difference with respect to vertical polarization is 11.76%. In the case of horizontal polarization, a similar trend is observed, with the percentage difference of 18.99% at the same diameter. The lower percentage difference is recorded in the M-C model against the Mie model. At a diameter of 2 mm, the percentage differences between the M-C model and the Mie model are 5.60% and 12.23% for vertical and horizontal polarization, respectively. At a frequency of 245.5 GHz, in Figure 2f, the same trend is observed as was the case for the lower frequency (7.8 GHz). The percentage difference at the 245.5 GHz frequency is approximately twice the values reported at the lower frequency.

5. SPECIFIC AND TOTAL RAIN ATTENUATION

The prediction of rainfall attenuation is achieved through the numerical integration of the following equation:

$$A = 4.34\times10^{-3}\int_0^{D_{max}} Q_{ext}(D)N(D)dD \quad (22)$$

where $Q_{ext}(D)$ represents the extinction cross section as given in equation (22) above. *N(D)* is the mean drop size distribution of the rainfall drops given by equations (8) and (9). The impact of distorted raindrops on attenuation due to rain is determined for the P-P model, M-C-model, and Mie model for frequencies up to 100 GHz. The results are plotted on the same set of axes for ease of comparison. As indicated in section 4.2, comparisons are made by using different total scattering cross-section models at circular polarization to determine specific rain attenuation as shown in Figure 3. The choice of circular polarization is considered because of its popularity in satellite communications at SHF and EHF ranges. In order to investigate the variability of specific rain attenuation, a single rain rate has been chosen from each rainfall regime to show the degree of the attenuation impact on the link operating at a given frequency, as shown in Figures 3 (a) to 3(d).

To highlight the worst case scenarios, the upper band of rain rate values are used for each rain type, namely: 5 mm/h, 10 mm/h, 40 mm/h, and 100 mm/h for drizzle, widespread, shower, and thunderstorm rain types, respectively. The percentage difference between the specific attenuation due to Mie model and that due to the M-C model is high compared to the difference due to the Mie and the P-P models. The highest average percentage difference in specific attenuation is thus obtained for the thunderstorm rain type with the M-C model, giving a value of 31.47%; while its P-P model counterpart gives a

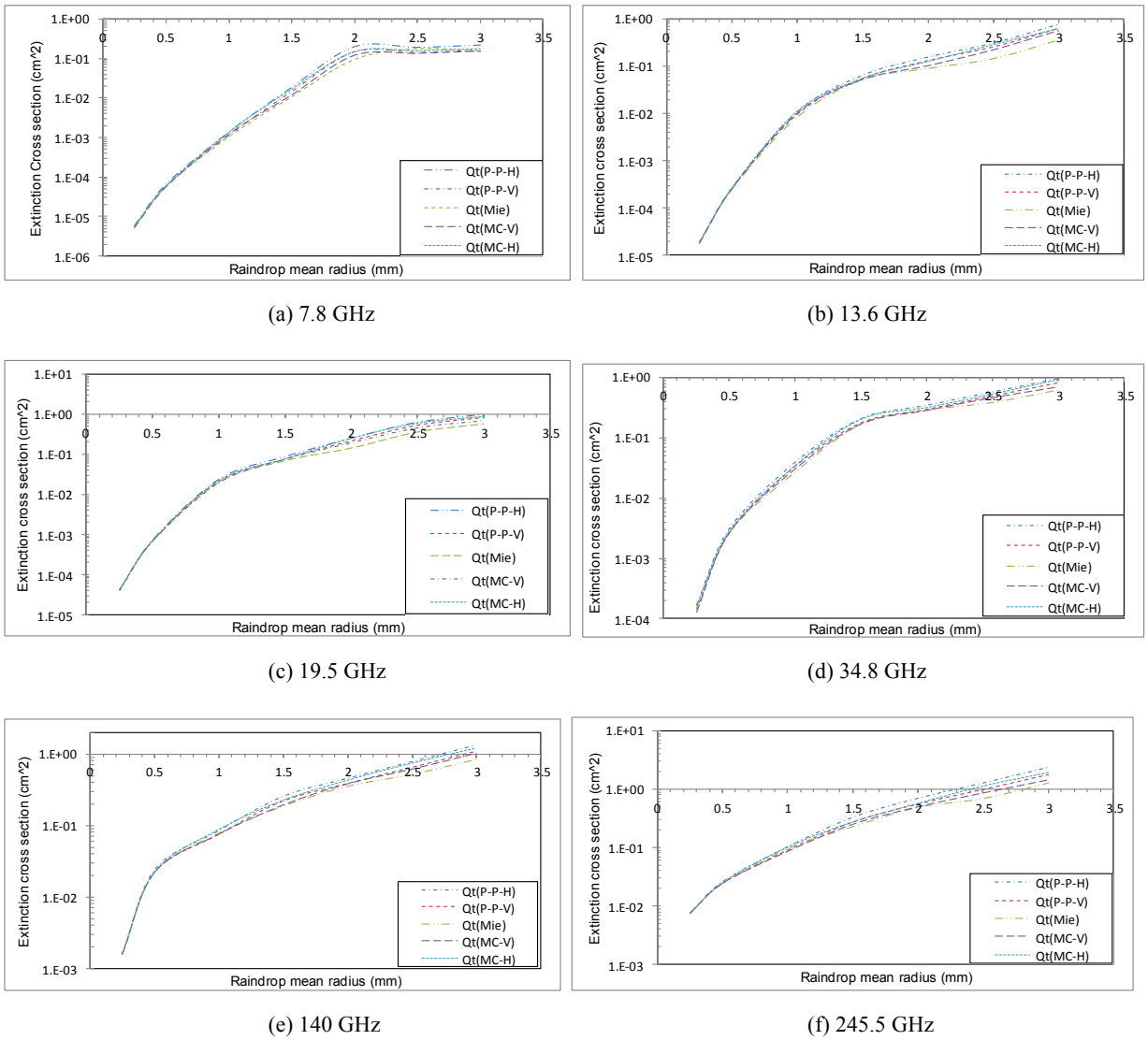

(a) 7.8 GHz (b) 13.6 GHz

(c) 19.5 GHz (d) 34.8 GHz

(e) 140 GHz (f) 245.5 GHz

Figure 2: Comparison of extinction cross-sections of MC, P-P, and Mie models at horizontal and vertical polarization versus mean drop radius at (a) 7.8 GHz (b) 13.6 GHz (c) 19.5 GHz (d) 34.8 GHz (e) 140 GHz (f) 245.5 GHz

difference of 30.95%. The lowest difference in specific attenuation is observed with the drizzle rain type, returning values of 9.27% and 15.11% between the Mie and the P-P model and the Mie and the M-C model, respectively.

The specific attenuation due to rain in an area gives the radio planner information about the extent to which the transmitted signal will be degraded in the presence of rain. The choice of operating frequency of a radio link is influenced by the rain attenuation and availability stipulations for the service on offer. Figure 3 shows the specific rain attenuation for a radio link operating at frequencies of up to 100 GHz for four different rain types. It is clear that the severity of signal degradation increases with increasing frequency. This translates into higher fade margin requirements at high frequencies to ensure reliable service for radio link users. Of the three models used in this study, the Mie model stipulates lower fade margin demands at all frequencies, while the M-C model calls for the highest fade margin requirements for all frequencies. The P-P model gives fade margins that lie in between these two.

Considering the specific attenuation due to different rain types described in section 2, we can see that the three models are in reasonably good agreement as shown in Fig. 3(a) for the drizzle rain type. The drizzle rain type is characteristically dominated by small rain drops and rain rate of at most 5 mm/h. This is in keeping with the notion that small rain drops are almost spherical in shape. The effective raindrop radius, a_e, of the P-P and M-C models, reduces to nearly that of the spherical model, giving almost the same attenuation levels as those due to the Mie model. However, as the raindrop size increases, the difference in the results from the three models becomes more noticeable. A summary of the percentage

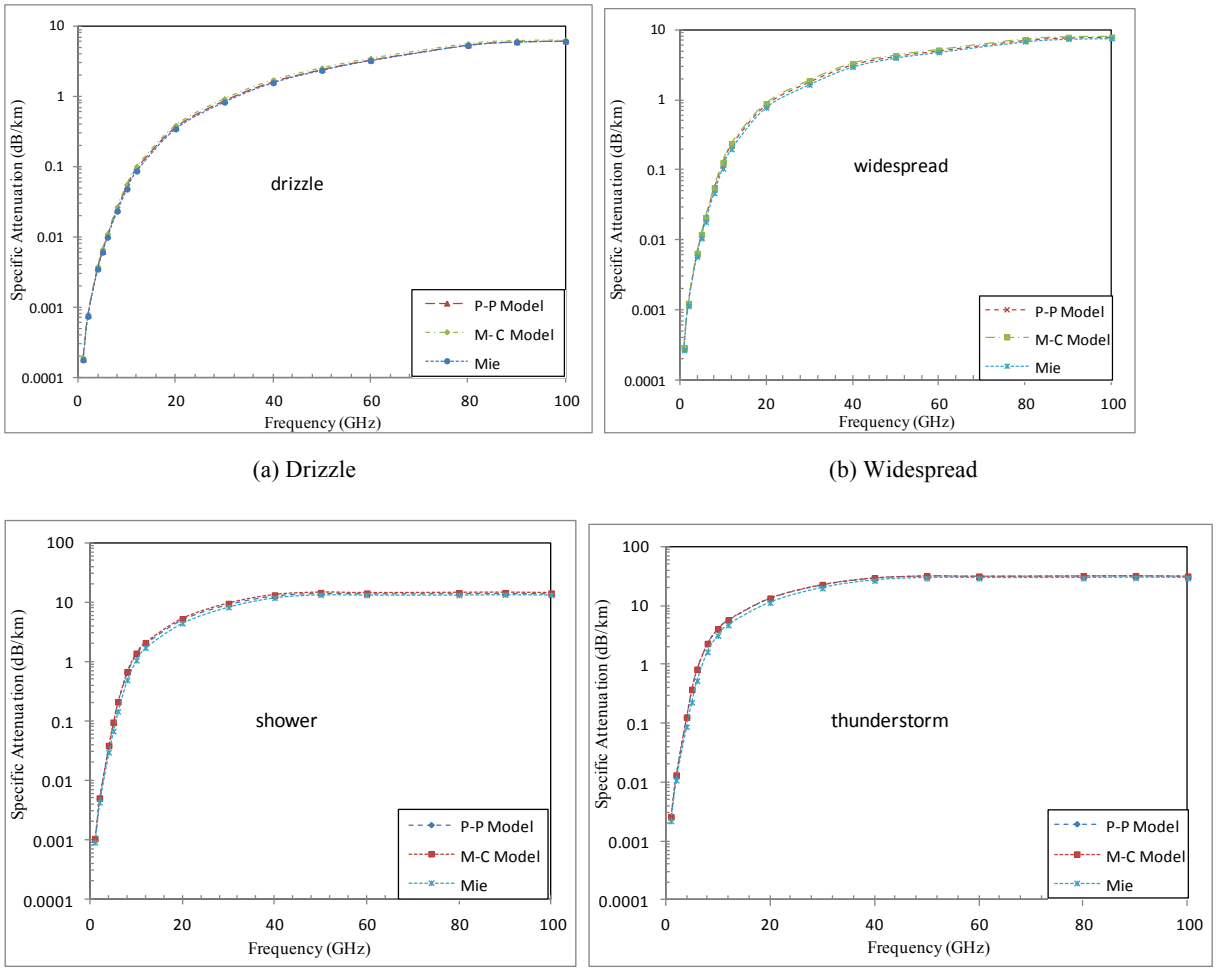

(a) Drizzle (b) Widespread

(c) Shower (d) Thunderstorm

Figure 3: Specific attenuation due to rain versus frequency for different rain types: (a) Drizzle, (b) Widespread, (c) Shower and (d) Thunderstorm

differences in specific attenuation between the P-P and M-C models on the one hand, with the Mie model on the other, is shown in Table 3. The comparison is made at the frequency of 100 GHz. More importantly, this comparison gives insight into the validity of the widely accepted Mie model.

The positive values in the table indicate that the values obtained using the Mie model are less than those of its counterparts. Table 3 clearly indicates that the difference between the values obtained using the Mie model and its counterparts increase with increasing rain rate.

The specific attenuation due to rain varies considerably with operating frequency. Figures 4(a) to 4(d) show how the specific rain attenuation varies with rain rate for the three models. For both the M-C and the P-P models, the plotted graphs are presented for both vertical and horizontal polarizations. The effect of raindrop distortion is investigated once more and compared with the spherical model of Mie. The results presented in Table 3 represent the average percentage differences in specific attenuation between the Mie model and its two counterparts for several frequencies in the range $1 \leq f \leq 245.5$ GHz. It is seen from Table 4 that the percentage difference of specific attenuation decreases with increasing frequency. The highest percentage difference of 35.90% is obtained between the Mie model and the P-P model, while a difference of 28.85% is obtained between the Mie model and the M-C model at 7.8 GHz. On the other hand, the lowest percentage difference is observed at a frequency of 140 GHz, with values of 0.81% and 1.04 % for the M-C model (vertical polarization) and the P-P model (vertical polarization), respectively. All the values in Table 4 are determined for an extreme rain rate of 100 mm/h. This result is more evident in Fig. 3, where small gaps between the graphs are noticeable at lower frequencies. At high frequencies, the graphs seem to attain close values. This implies that the three models are in reasonably good agreement at high frequencies. The Mie model thus gives a good representation of the drop shape even at high frequencies, while a considerable difference is observed at lower frequencies.

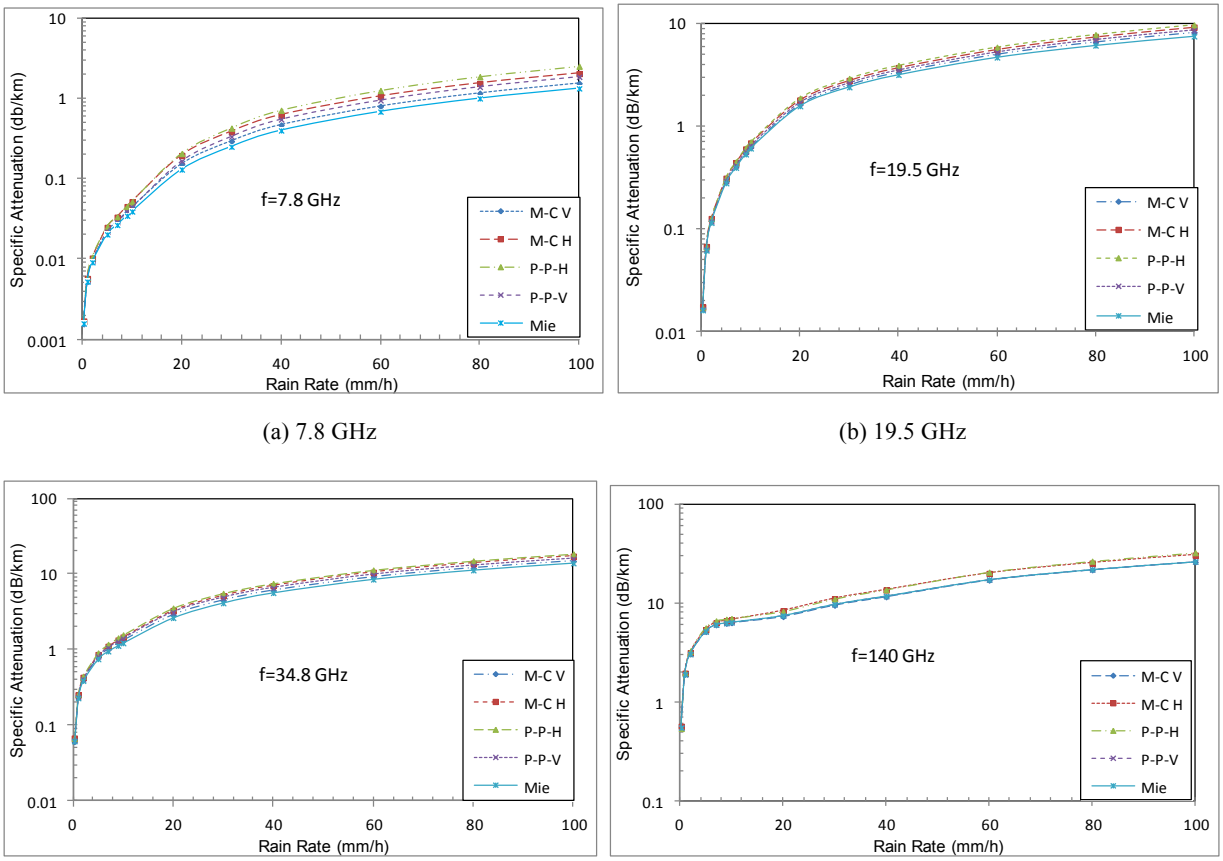

(a) 7.8 GHz (b) 19.5 GHz

(c) 34.8 GHz (d) 140 GHz

Figure 4: Specific rain attenuation against rain-rate for (a) 7.8 GHz (b) 19.5 GHz (c) 34.8 GHz and (d) 140 GHz

6. THE kR^{α} RAIN ATTENUATION MODEL

The ITU-R recommends the use of the power law relationship given by equation (1) to determine the specific attenuation due to rain, provided the local rain rate is known. In this paper, the results of specific rain attenuation obtained using the Lognormal DSD are modelled using the power law relationship. As mentioned earlier on, the coefficients k and α vary with both frequency and location-dependent rain drop size distribution. These coefficients are determined and presented in Table 5 for Durban, which lies on the east coast of South Africa. In this section circular polarization is assumed. Once again, three raindrop size models are considered, one being the popular spherical drop shape of Mie, while the other two take into account distortion during the drop fall. The power law model parameters are presented in Table 5 with subscripts m, p, and s representing Mie, P-P, and M-C models respectively.

Figure 6 shows the parameter α modelled for the frequency range $1 \leq f \leq 10$ GHz and $10 < f \leq 100$ GHz. The results in Table 6 and 7 can be used to determine the power law coefficients at any desired frequency in the range $1 \leq f \leq 100$ GHz. The specific rain attenuation can thus be determined at all frequencies in this range of desired rain rates. The following general model is realized:

$$k = A_1 f^4 + B_1 f^3 + C_1 f^2 + D_1 f + E_1 \quad (23)$$

$$\alpha = A_2 f^4 + B_2 f^3 + C_2 f^2 + D_2 f + E_2 \quad (24)$$

where A_1 and A_2 represent the fourth coefficient of the polynomial, B_1 and B_2 represent the third coefficient, C_1 and C_2 represent the second coefficient, D_1 and D_2 represent the first coefficient, and E_1 and E_2 represent the constant of the polynomial. Substituting the coefficients shown in Table 6 and 7 into equation (23) and (24) enables the determination of k and α for different frequencies.

7. CONCLUSION

This paper presents realistic raindrops based on their extinction total cross section and the specific attenuation due to rain using three models, namely, the M-C (or spheroidal) model, the P-P model, and the Mie (or spherical) model. The paper further investigates the validity of the Mie spherical raindrops model that is used

Table 4: Comparison of the P-P and M-C models to the Mie model at different frequencies

Frequency (GHz)	Average Attenuation Percentage difference (%)			
	P-P V Model	P-P H Model	M-C V Model	M-C H Model
7.8	17.36	35.90	10.20	28.85
13.6	9.19	18.00	10.25	19.04
19.5	7.26	15.80	4.79	13.32
34.8	10.99	22.59	5.67	17.25
140	1.04	10.47	0.81	8.46
245.5	2.47	13.55	1.71	9.18

Table 5: Power law model parameters for the three drop-size models

Frequency (GHz)	Mie Model		P-P Model		M-C Model	
	k_m	α_m	k_p	α_p	k_s	α_s
1	0.00006	0.7595	0.00006	0.7759	0.00006	0.7758
2	0.0002	0.7836	0.0002	0.8043	0.0002	0.8040
4	0.001	0.8663	0.001	0.9064	0.001	0.9039
5	0.0016	0.9239	0.0016	0.9776	0.0017	0.9779
6	0.0025	0.9859	0.0025	1.0500	0.0026	1.0448
8	0.0052	1.0797	0.0053	1.1319	0.0056	1.1291
10	0.0099	1.1168	0.0103	1.1574	0.0109	1.1562
12	0.0172	1.1180	0.0179	1.1442	0.019	1.1424
20	0.0714	1.0471	0.0736	1.0667	0.0776	1.0636
30	0.1914	0.9692	0.1975	0.9835	0.2088	0.9807
40	0.382	0.9145	0.3928	0.9239	0.4137	0.9208
50	0.6226	0.8427	0.6364	0.8489	0.6682	0.8441
60	0.929	0.7638	0.9477	0.7687	0.9951	0.7637
80	1.6774	0.6631	1.7026	0.6692	1.7705	0.6672
90	1.9331	0.6412	1.954	0.6471	2.014	0.6459
100	2.053	0.6266	2.0686	0.6325	2.1186	0.6319

Table 6: Modelled coefficient *k*

Fit Model		Mie	P-P	M-C
Fourth Order Polynomial $1 \le f \le 100$ GHz	4^{th}	-7E-8	-7E-8	-7E8
	3^{rd}	1E-5	1E-5	1E-5
	2^{nd}	-1E-4	-1E-4	-1E-4
	1^{st}	3.3E-3	3.3E-3	3.2E-3
	constant	-0.0114	-0.0115	-0.0113

by many researchers. It is observed that while the extinction cross-section varies considerably with raindrop size, the three models show a close agreement for small raindrop diameters but differ as the drop size increases. The Mie model thus remains accurate for fade margin determination for small raindrop diameters; this model therefore gives reliable specific rain attenuation predictions in regions dominated by drizzle rainfall, but will considerably underestimate the attenuation in regions dominated by shower and thunderstorm rain types.

The results also show that the raindrop extinction cross section for the three models agree at the lower frequencies while as the frequency increases, a noticeable difference is observed. The effect of polarization is noticed in the M-C model and the P-P model, with the horizontal polarization returning the higher percentage difference compared to the Mie model.

The specific attenuation due to rain for different total cross-sections (P-P, M-C and Mie models) with circular polarization for different rain types shows a progressive increase in the average percentage differences (with respect to the Mie model) from drizzle through widespread to thunderstorm. The average specific attenuation percentage difference for the P-P model is low compared to the M-C model. The results further show that the power law model parameters, k and α, can be modelled using the fourth order polynomial as shown by equations (23) and (24). The specific rain attenuation can thus be determined using the power law model for frequencies up to 100 GHz and rain rate up to 100 mm/h. In regions where there is a high presence of large raindrops (as is the case in tropical and sub-tropical regions like South Africa), it is inadequate to employ the Mie model in the determination of local rain fade margins. However, this model is acceptable for regions dominated by the drizzle rain type due to a high presence of small drops.

8. REFERENCES

[1] International Telecommunication Union Radio communication (ITU-R), "Specific attenuation model for rain for use in prediction methods", Recommendation ITU-R P.838.3, *International Telecommunication Union*, Geneva, Switzerland, 2005.

[2] G.O. Ajayi and R.L.Olsen, "Modelling of a tropical raindrop size distribution for microwave and millimeter wave applications," *Radio Science,* Vol. 20, Issue 2, pp. 193–202, March-April 1985.

[3] F. Moupfouma, "A new theoretical formulation for calculation of the specific attenuation due to precipitation particles on terrestrial and satellite radio links," *International Journal of Satellite Communications*, Vol. 15, pp. 89-99, 1997.

[4] I. Seishiro, "Rain attenuation at millimeter wavelength of 1.33 mm," *International Journal of Infrared and Millimeter waves*, Vol. 25, No.10, pp. 1495-1501, October 2004.

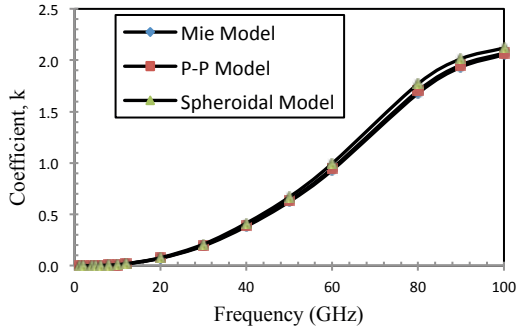

Figure 5: Coefficient *k* against frequency (Note: the Spheroidal model is the M-C model)

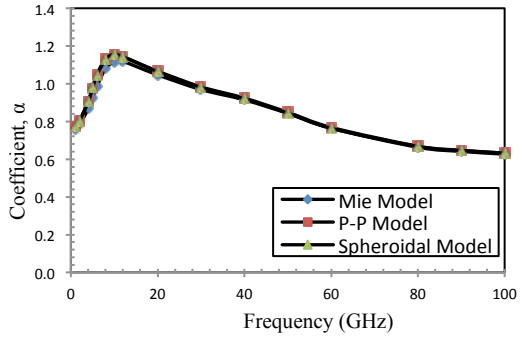

Figure 6: Coefficient α against frequency (Note: the Spheroidal model is the M-C model)

Table 7: Modelled coefficient α

Polynomial Fit		Mie	P-P	M-C
4th Order Polynomial 1 ≤ f ≤ 10 GHz	4th	-	8E-5	8E-5
	3rd	-9E-4	-2.8E-	-2.7E-3
	2nd	1.43E-	2.81E-	2.76E-
	1st	-1.65E-	-4.4E-	-4.28E-
	constant	0.7638	0.7964	0.7954
3rd Order Polynomial 10 < f ≤ 100 GHz	3rd	5E-7	4E-7	4E-7
	2nd	-4E-5	-3E-5	-2E-5
	1st	-6.3E-3	-7.6E-	-7.7E-3
	constant	1.1923	1.232	1.232

[5] J.O. Laws and D.A. Parsons, "The relation of raindrop size to intensity," *Transactions, American Geophysical Union*, Volume 24, Issue 2, pp. 452-460, 1943.

[6] K.I. Timothy, J.T. Ong and E.B.L. Choo, "Raindrop Size Distribution Using Method of Moments for Terrestrial and Satellite Communication Applications in Singapore," *IEEE Transactions on Antennas and Propagation*, Vol. 50, No.10, pp. 1420-1424, October 2002.

[7] H. Jiang, M. Sano, and M. Sekine, "Weibull raindrop size distribution and its application to rain attenuation," *IEE Proc. Microwave and Antennas Propag*. Vol. 144, No.3, pp. 197-200, June 1997.

[8] M. Sekine, C. Chen, and T. Musha, "Rain attenuation from log-normal and Weibull raindrop-size distributions," *IEEE Trans. Antenna and propagation,* Vol. AP-35, No.3, pp. 358-359, March 1987.

[9] D.A. De Wolf, "On the Law-Parsons distribution of raindrop sizes," *Radio Science*, Vol. 36, No.4, pp. 639-642, June/August 2001.

[10] T.Kozu, *Estimation of raindrop size distribution from space borne radar measurements.* Ph.D. dissertation, Univ.of Kyoto, Japan, 1991.

[11] P.W. Mielke Jr., "Simple iterative procedures for two parameter gamma distribution maximum likelihood estimates," *J. Appl. Meteor*. Vol. 15, pp. 181-183, 1976.

[12] S. Moumouni, M. Gosset, and E. Houngninou, "Main features of rain drop size distributions observed in Benin, West Africa, with optical distrometers," *Geophysical Research Letters*, Vol. 35, No. 23, L23807, doi: 10.1029/2008GL035755, December 2008.

[13] P.A. Owolawi, "Raindrop Size Distribution Model for the Prediction of Rain Attenuation in Durban," *PIERS*, Vol. 7, No.6, pp. 51-523, 2011.

[14] T.J.O. Afullo, "Raindrop Size Distribution Modelling for Radio Link Design along the Eastern Coast of South Africa," *PIER B*, Vol.34, pp. 345-366.

[15] J.A Morrison and M.J. Cross, "Scattering of a plane electromagnetic wave by axisymmetric raindrops," *Bell Syst. Tech, J.*, Vol. 53, pp. 955-1019, July-August, 1974.

[16] H.R. Prupacher, and R.L. Pitter, "A semi-empirical determination of shape of cloud and rain drops," *J. Atmos. Science,* Vol. 28, pp. 86-94, 1971.

[17] L.W. Li, P.S. Kooi, M.S. Leong, , T.S. Yeo, and M.Z. Gao, "Microwave attenuation by realistically distorted raindrops: Part I-Theory," *IEEE Trans. Antenna Propagation,* Vol. 43, No.8., pp. 811-821, 1995.

[18] L. W. Li, P. S. Kooi, M. S. Leong, and T. S. Yeo, "Integral Equation Approximation to Microwave Specific Attenuation by Distorted Raindrops: The Pruppacher-and-Pitter Model," *Proceedings of IEEE Singapore International Conference*, 3-7 Jul 1995, pp. 600-604, ISBN: 0-7803-2579-6.

[19] L. W. Li, P. S. Kooi, M. S. Leong, and T. S. Yeo, "Integral Equation Approximation to Microwave Specific Attenuation by Distorted Raindrops: The Spheroidal Model," *Proceedings of IEEE Singapore International Conference,* 3-7 Jul 1995, pp. 658-662, ISBN: 0-7803-2579-6.

[20] T. Oguchi, "Attenuation of electromagnetic wave due to rain with distorted raindrops," *J. Radio Res. Labs*., Vol. 7, pp. 467-485, 1960.

[21] Distromet Ltd., *Distrometer RD-80 instructional manual*, Basel, Switzerland, June 20, 2002.

[22] I.A. Adimula and G.O. Ajayi, "Variation in drop size distribution and specific attenuation due to rain in Nigeria," *Annales Des Télécommunications*, Vol. 51, Issue 1-2, pp. 87-93, Jan-Feb 1996.

[23] S.J. Malinga and P.A. Owolawi, "Obtaining raindrop size model using method of moment and its applications for South Africa radio systems," *PIER B*, Vol.46, pp. 119-138, 2013.

[24] T.J. Schuur, A.V. Ryzhkov, D.S. Zrnic, and M Schonhuber, "Drop Size Distribution Measured by a 2D Video Disdrometer: Comparison with Dual-Polarization Radar Data," *Journal of Applied Meteorology*, Vol. 40, pp. 1019 – 1034, June, 2001.

[25] H. R. Pruppacher and K. V. Beard, "A wind tunnel investigation of the internal circulation and shape of water drops falling at terminal velocity in air," *Quart. J. R. Met. Soc*., Vol. 96, pp. 247-256, April 1970.

[26] T. Oguchi, "Electromagnetic wave propagation and scattering in rain and other hydrometeors," *Proc. IEEE*, Vol. 71, Issue 9, pp. 1029-1078, Sept. 1983.

[27] L. W. Li, P. S. Kooi, M. S. Leong, and T. S. Yeo, "On the simplified expression of realistic raindrop shapes," Microwave & Optical Technol. Letters, Vol. 7, Issue 4, pp. 201–205, March 1994